Vertical profiles of NO_3 reactivity within the surface layer of a boreal forest

Patrick Dewald[1], Simone T. Andersen[1], Gunther N. T. E. Türk[1], Laura Wüst[1], Carolina Nelson[1], Jan Schuladen[1], Mikael Ehn[2], Tuukka Petäjä[2], Ilona Ylivinkka[2,3], Lauri R. Ahonen[2,3], Horst Fischer[1], Jos Lelieveld[1], and John N. Crowley[1]

[1]Atmospheric Chemistry Department, Max Planck Institute for Chemistry, 55128 Mainz, Germany
[2]Institute for Atmospheric and Earth System Research/Physics, Faculty of Science, University of Helsinki, Helsinki, Finland
[3]Station for Measuring Ecosystem - Atmosphere Relations II (SMEAR II), University of Helsinki, Korkeakoski, 35500, Finland

Correspondence to: John N. Crowley (john.crowley@mpic.de)

Supplementary Information

S1 Comparison between NO_3 reactivity and monoterpene measurements

During the BAIRN-VIP campaign, a proton-transfer reaction time-of-flight mass spectrometer (PTR-ToF-MS) monitored the sum of monoterpenes (ΣMTs) atop the tower. In Fig. S1, we plot the VOC-induced NO_3 reactivity (with $k^{VOC} > LOD$) measured at 28 m against the monoterpene concentrations monitored at 36 m. To reduce bias caused by vertical gradients we analyse only daytime data between 09:00 and 17:00 UTC.

A weighted, orthogonal distance regression yields a slope of 5.6×10^{-12} cm^3 molecule^{-1} s^{-1} and an intercept of -0.004 s^{-1}. The absolute value of the intercept is below the LOD of the CRDS setup and thus not significant. The slope is the mean effective reaction rate coefficient (k_{eff}) for the reaction of NO_3 with VOCs and is consistent with that derived from a limited set of speciated monoterpene data (see Andersen *et al.*[1] for details).

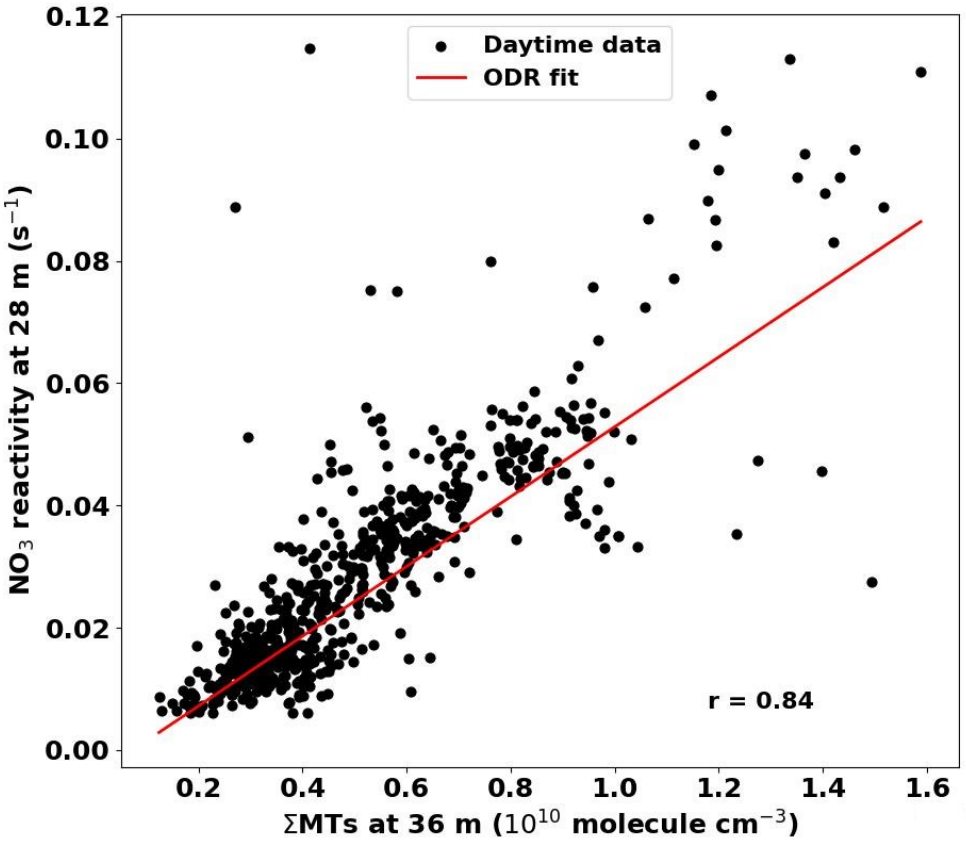

Figure S1: VOC-induced NO_3 reactivity (black circles) at 28 m plotted against the summed monoterpene concentration (ΣMTs) at 36 m at daytime during the BAIRN-VIP campaign. The red line shows a linear, orthogonal distance regression (weighted ODR fit) to the data. The Pearson correlation coefficient of 0.84 indicates a good correlation between these two measurements.

S2 Calculation of the vertical decoupling parameter Ω

The vertical coupling between the air above and below the forest canopy was assessed with the decoupling parameter Ω as introduced by Peltola *et al.*[2]. The key steps to calculate Ω are reproduced here, and the parameters used (or calculated) are plotted in Figure S2. We used the site-specific parameters for SMEAR II as detailed in Peltola *et al.*[3]. Ω is defined as the ratio of the standard deviation of vertical wind speed $\sigma_{\mathrm{w}}(z)$ to the absolute critical vertical wind speed $\left|w_{\mathrm{e,crit}}(z)\right|$ required to move an air parcel from a measurement height z above the canopy (here 27 m) to the ground. In order to achieve this, the air parcel must overcome both buoyancy and canopy drag. According to Eq. S1 as derived by Peltola *et al.*[2], the critical wind speed at canopy height h is

$$w_{\mathrm{e,crit}}(h) = -C\widehat{c_{\mathrm{d}}}LAIU_h - \sqrt{C^2\widehat{c_{\mathrm{d}}}^2LAI^2U_h^2 + 2gh\frac{\theta_{\mathrm{e}}-\bar{\theta}}{\bar{\theta}}} \quad \text{(S1)}$$

with g = 9.81m s^{-2} and site-specific parameters for SMEAR II as detailed in Peltola *et al.*[3], i.e. h is 21 m, leaf area index LAI is 2 m^2 m^{-2}, the constant C is 0.277, and the drag coefficient $\widehat{c_{\mathrm{d}}}$ is 0.2. The mean potential temperature below the canopy $\bar{\theta}$ as well as the potential temperature of the air parcel θ_{e} were derived from the absolute temperature measurements between 0.4 m and 27 m (see Fig.1 in the main text) at the mast and the dry adiabatic lapse rate of 9.68 x 10^{-3} K m^{-1}.[4] The horizontal wind speed was only measured above the canopy (U_z) at z = 27 m. To derive the horizontal wind speed at canopy height U_h, we applied the Monin-Obukhov similarity theory:[3, 5]

$$U_h = U_z - \frac{u^*\phi_{\mathrm{m}}}{k_{\mathrm{K}}(z-d)}(z-h) \quad \text{(S2)}$$

In Eq. S2, u^* is the friction velocity at z = 27 m, k_{K} is the von Kármán constant (0.4) and ϕ_{m} (Eq. S3) is the stability scaling function. Latter is defined as:

$$\phi_{\mathrm{m}} = \begin{cases} 1, & \zeta < 0 \\ 1 + 5\zeta, & \zeta > 0 \end{cases} \quad \text{(S3)}$$

with the Monin-Obukhov stability parameter $\zeta = \frac{z-d}{L}$, where d is the displacement height being approximated with $^2/_3\,h$ and L the Obukhov length measured at z = 27 m.[3, 6] The critical wind speed at measurement height z is derived from Eq. S4 with the mean potential temperature $\bar{\theta}'$ between z and h:

$$w_{\mathrm{e,crit}}(z) = \sqrt{w_{\mathrm{e,crit}}^2(h) + 2g(z-h)\frac{\theta_{\mathrm{e}}-\bar{\theta}'}{\bar{\theta}'}} \quad \text{(S4)}$$

Dividing the measured standard deviation in vertical wind speed by absolute $w_{e,crit}(z)$ results in Ω:

$$\Omega = \frac{\sigma_{\mathrm{w}}(z)}{|w_{\mathrm{e,crit}}(z)|} \quad \text{(S5)}$$

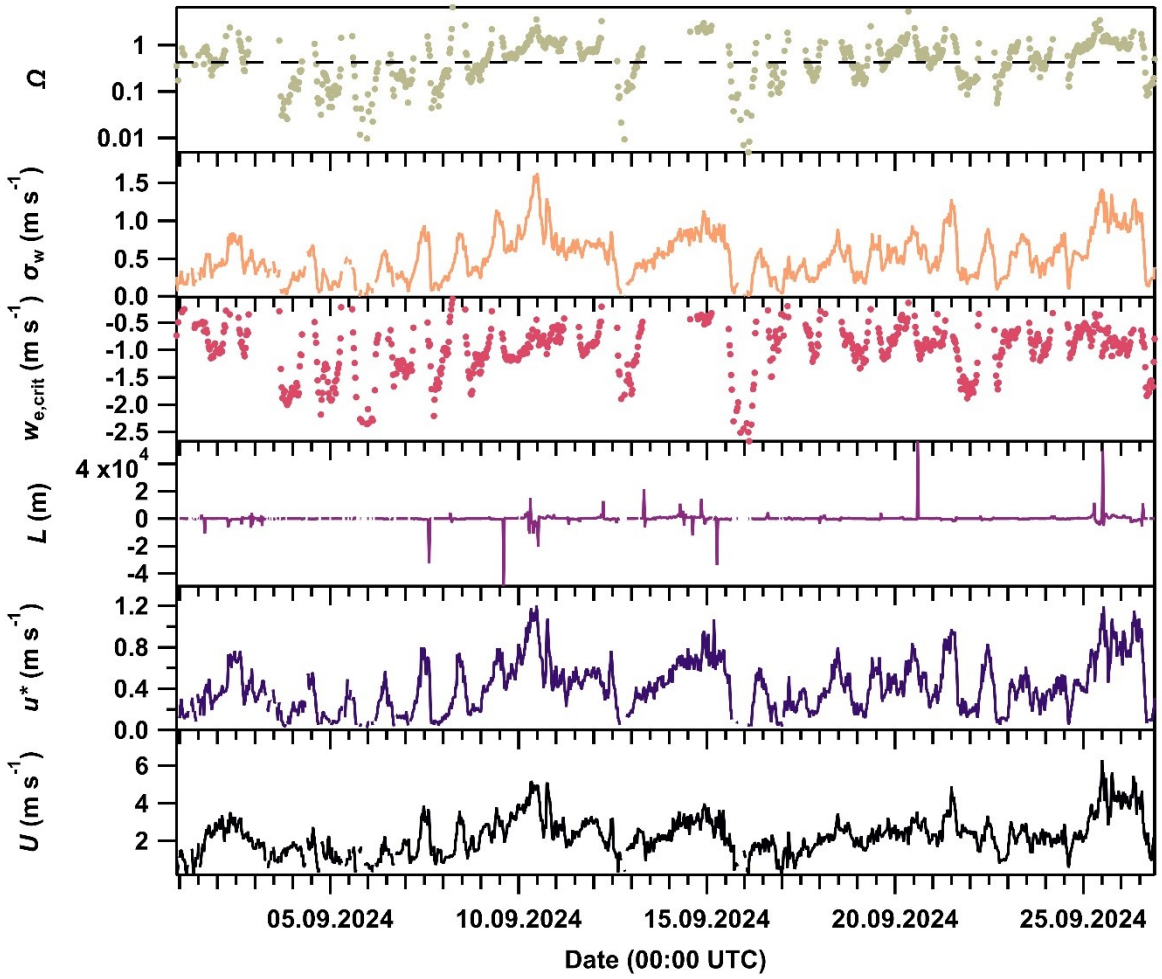

Figure S2: Measurements at SMEAR II site (z = 27 m) of horizontal wind speed U, friction velocity u*, Obukhov length L, standard deviation in vertical wind speed σ_w and calculated values of critical wind speed $\boldsymbol{w_{e,crit}}$ (Eq. S1–S4) and decoupling parameter Ω (Eq. 5) during the BAIRN-VIP campaign. The dashed line in the plot of Ω marks the threshold value of 0.43 for decoupled conditions.[2]

S3 Comparison between NO_3 photolysis frequencies and PAR below and above the canopy

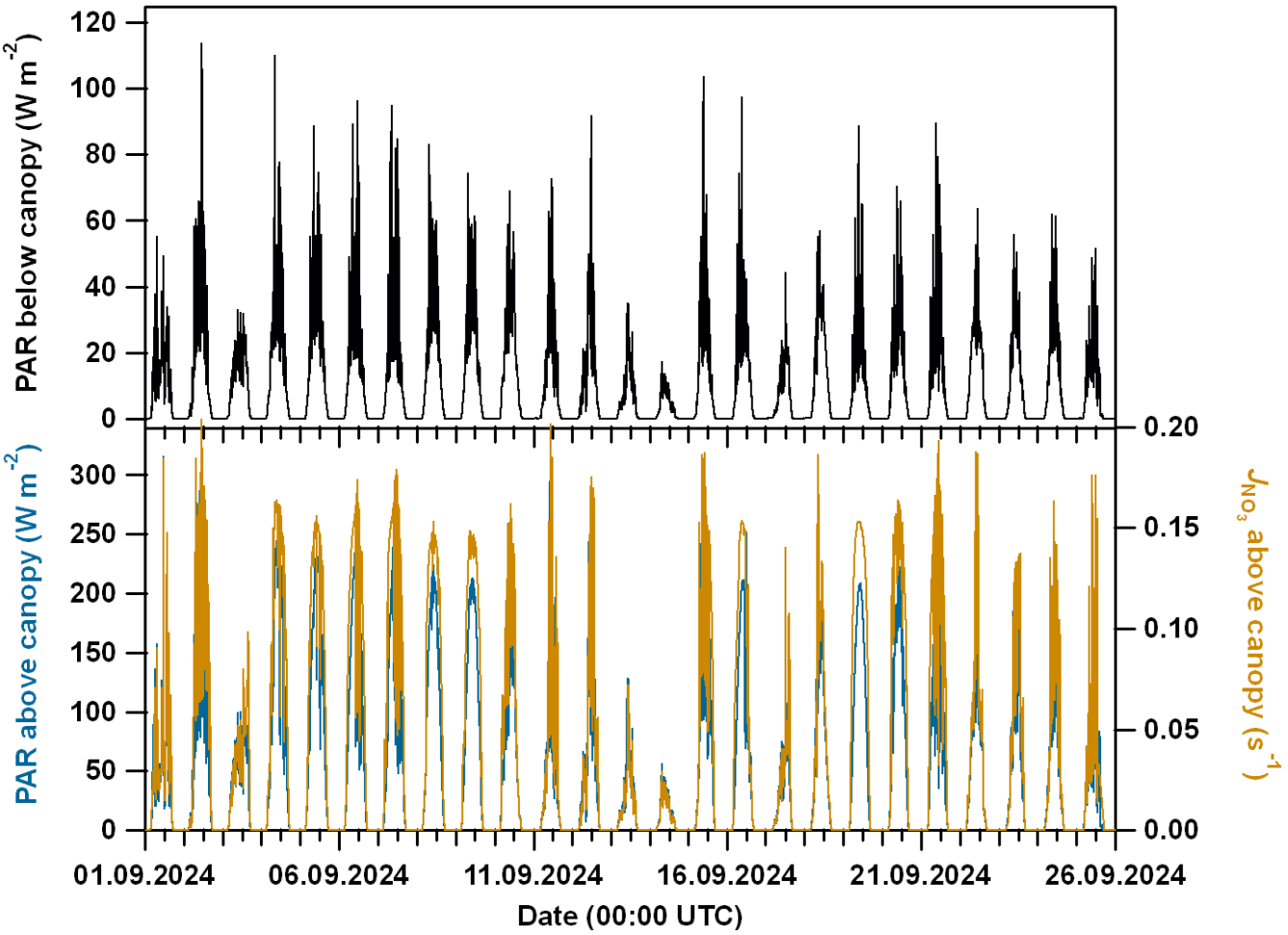

Figure S3: Photo-synthetically active radiation (PAR) measured in the forest at the SMEAR II site above the canopy (lower panel, blue, 35 m) and below the canopy (upper panel, black, 0.6 m). The NO_3 photolysis frequencies (J_{NO_3}) were derived from measurements on top of a tower adjacent to the forest clearing (lower panel, orange, 38 m).

S4 Vertical profiles in NO_3 reactivity and *f* on different nights

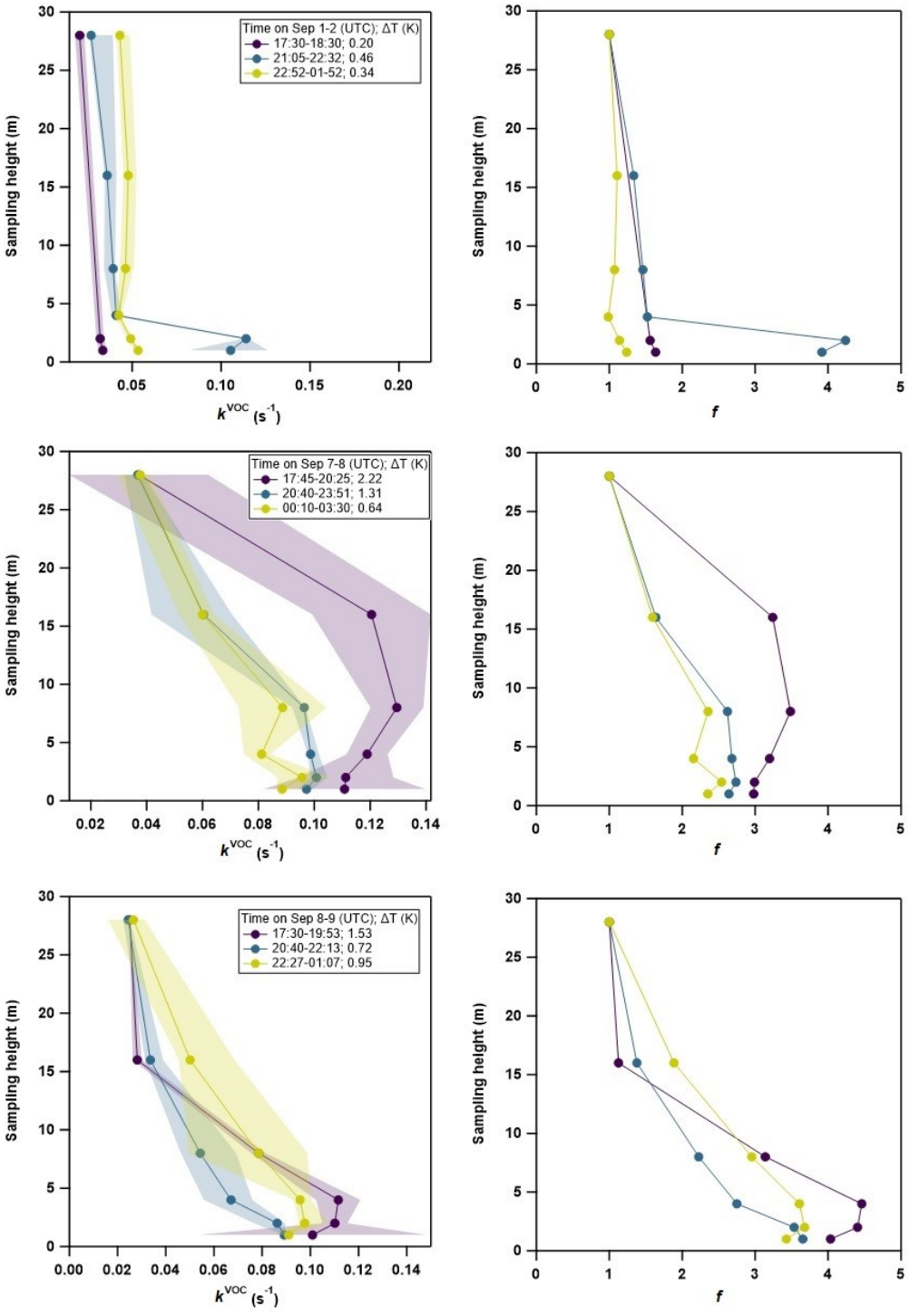

100

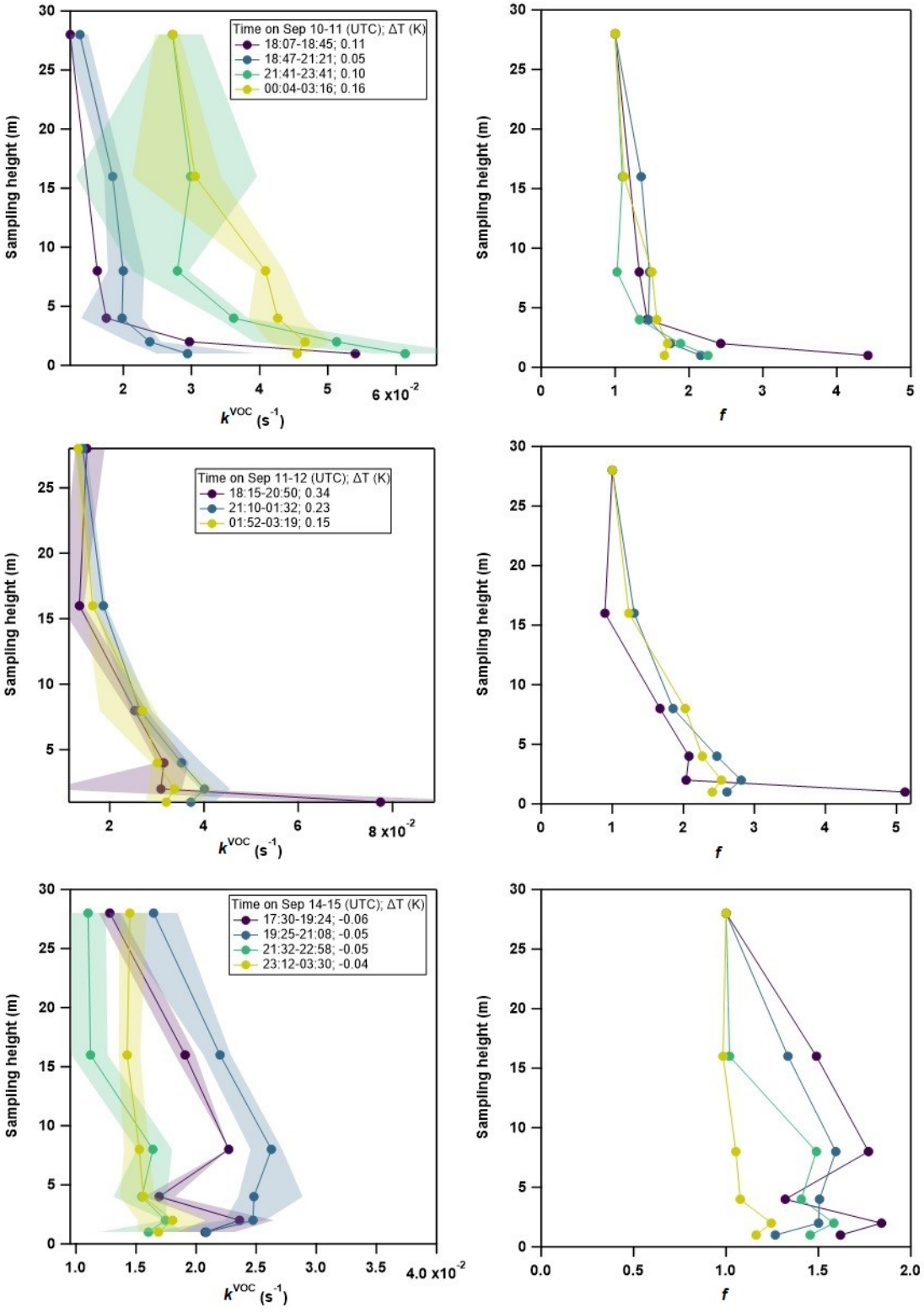
Time on Sep 10-11 (UTC); ΔT (K)
18:07-18:45; 0.11
18:47-21:21; 0.05
21:41-23:41; 0.10
00:04-03:16; 0.16
Time on Sep 11-12 (UTC); ΔT (K)
18:15-20:50; 0.34
21:10-01:32; 0.23
01:52-03:19; 0.15
Time on Sep 14-15 (UTC); ΔT (K)
17:30-19:24; -0.06
19:25-21:08; -0.05
21:32-22:58; -0.05
23:12-03:30; -0.04
Sampling height (m)
k^VOC (s^-1)
6 x10^-2
8 x10^-2
4.0 x10^-2
f

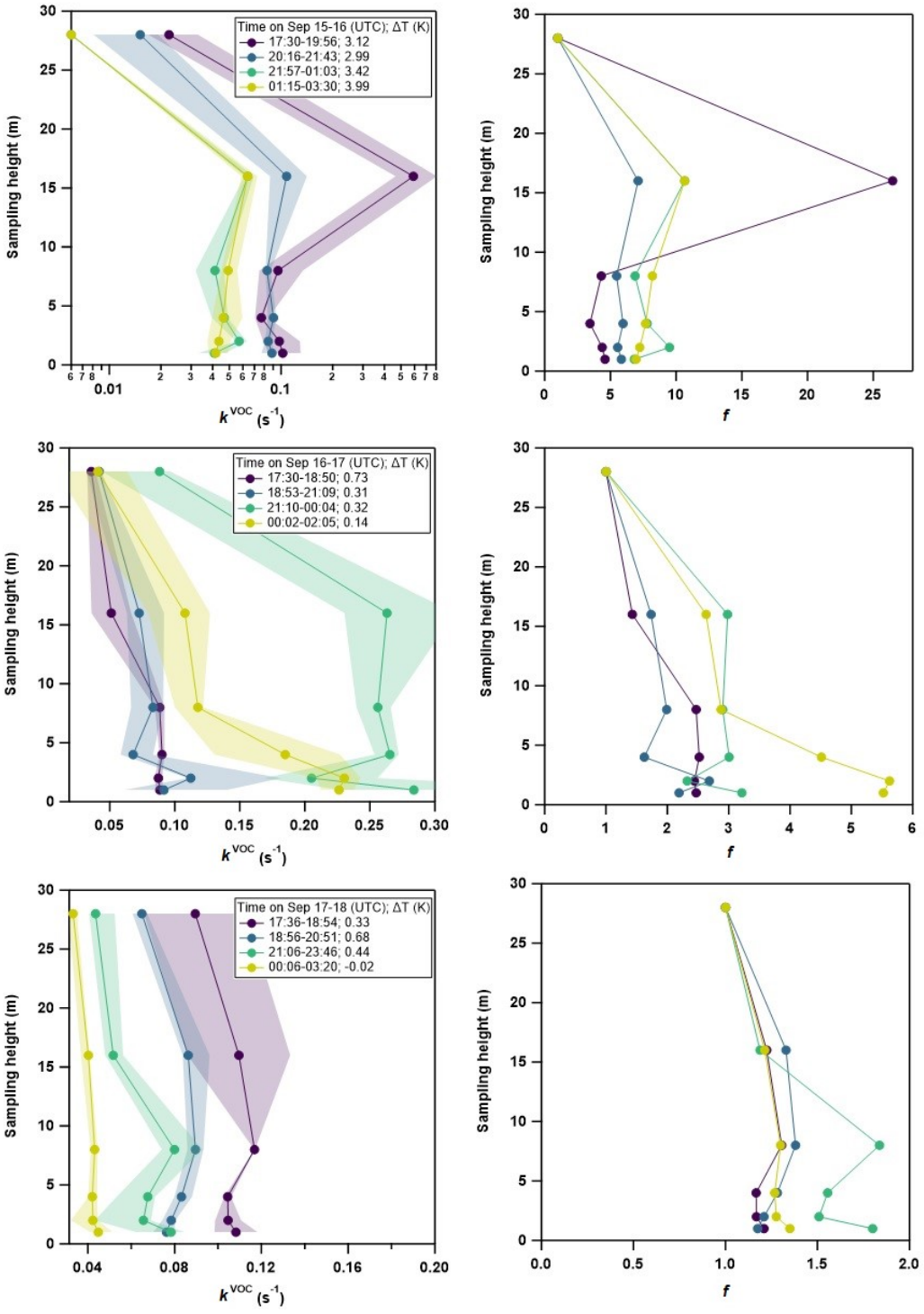
Time on Sep 15-16 (UTC); ΔT (K)
17:30-19:56; 3.12
20:16-21:43; 2.99
21:57-01:03; 3.42
01:15-03:30; 3.99
Sampling height (m)
k^{VOC} (s^{-1})
f
Time on Sep 16-17 (UTC); ΔT (K)
17:30-18:50; 0.73
18:53-21:09; 0.31
21:10-00:04; 0.32
00:02-02:05; 0.14
Sampling height (m)
k^{VOC} (s^{-1})
f
Time on Sep 17-18 (UTC); ΔT (K)
17:36-18:54; 0.33
18:56-20:51; 0.68
21:06-23:46; 0.44
00:06-03:20; -0.02
Sampling height (m)
k^{VOC} (s^{-1})
f

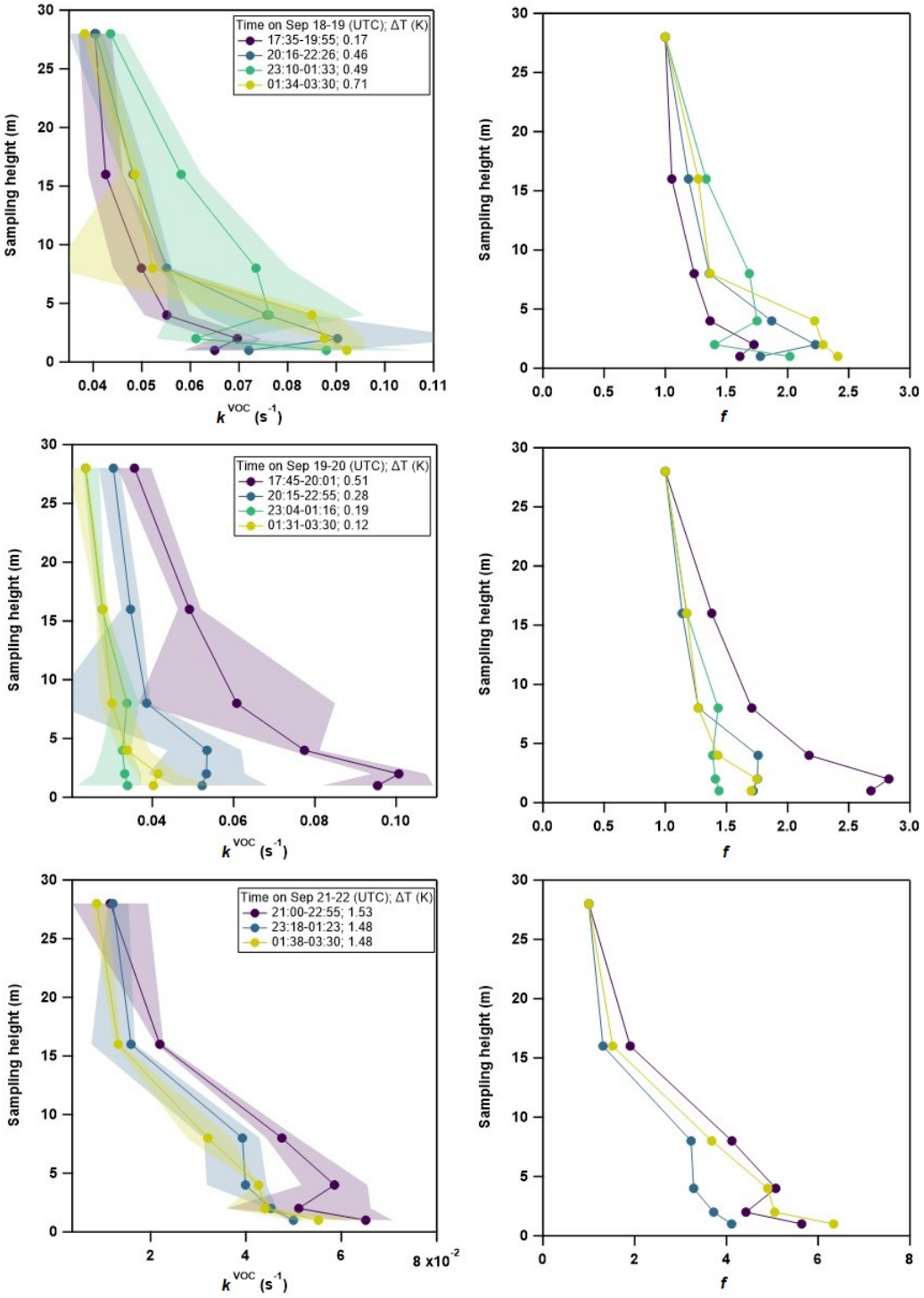
Time on Sep 18-19 (UTC); ΔT (K)
17:35-19:55; 0.17
20:16-22:26; 0.46
23:10-01:33; 0.49
01:34-03:30; 0.71
Sampling height (m)
k VOC (s-1)
f
Time on Sep 19-20 (UTC); ΔT (K)
17:45-20:01; 0.51
20:15-22:55; 0.28
23:04-01:16; 0.19
01:31-03:30; 0.12
Sampling height (m)
k VOC (s-1)
f
Time on Sep 21-22 (UTC); ΔT (K)
21:00-22:55; 1.53
23:18-01:23; 1.48
01:38-03:30; 1.48
Sampling height (m)
8 x10-2
k VOC (s-1)
f

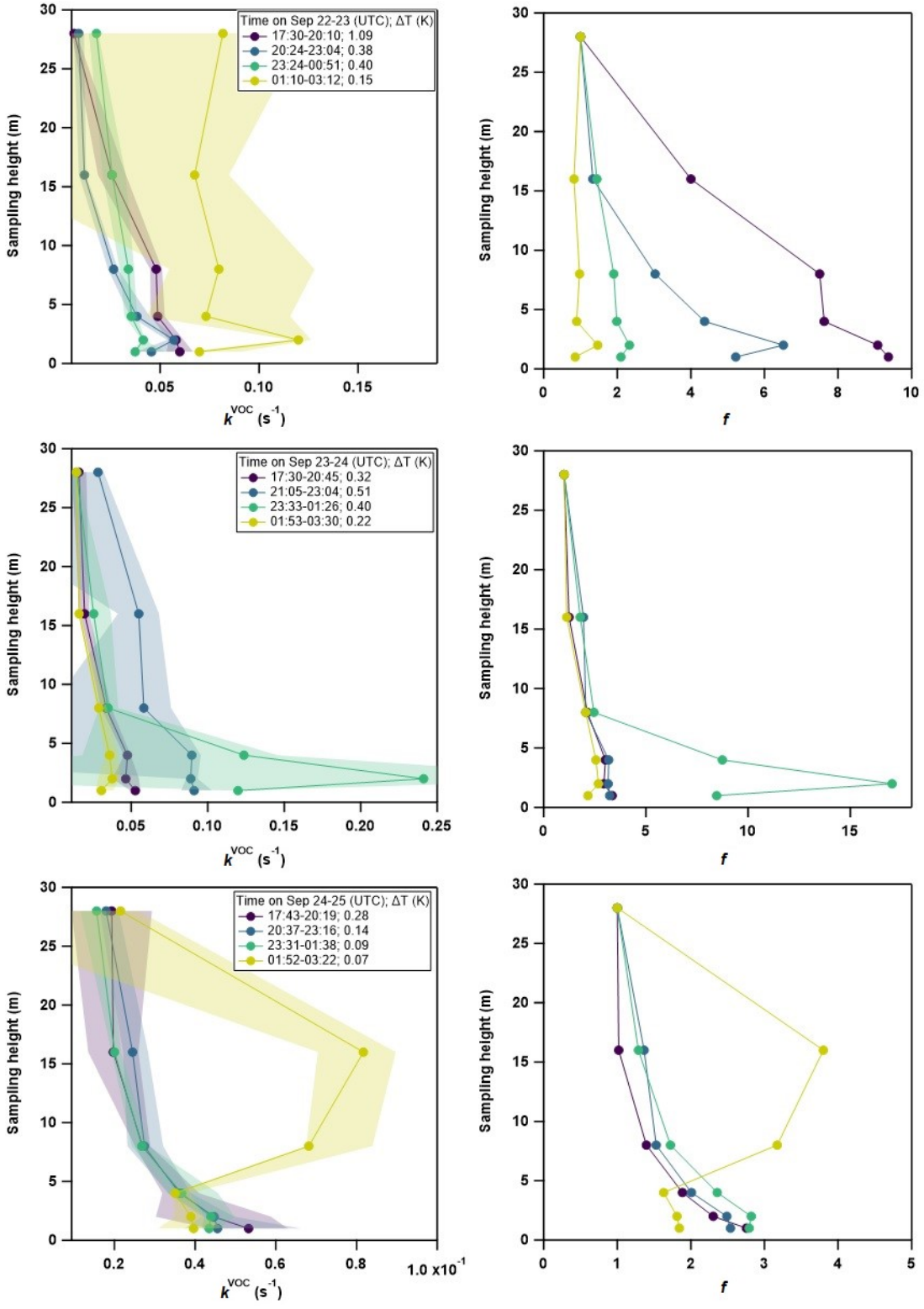
Time on Sep 22-23 (UTC); ΔT (K)
17:30-20:10; 1.09
20:24-23:04; 0.38
23:24-00:51; 0.40
01:10-03:12; 0.15
Sampling height (m)
k^{VOC} (s^{-1})
f
Time on Sep 23-24 (UTC); ΔT (K)
17:30-20:45; 0.32
21:05-23:04; 0.51
23:33-01:26; 0.40
01:53-03:30; 0.22
Sampling height (m)
k^{VOC} (s^{-1})
f
Time on Sep 24-25 (UTC); ΔT (K)
17:43-20:19; 0.28
20:37-23:16; 0.14
23:31-01:38; 0.09
01:52-03:22; 0.07
Sampling height (m)
k^{VOC} (s^{-1})
1.0 x10^{-1}
f

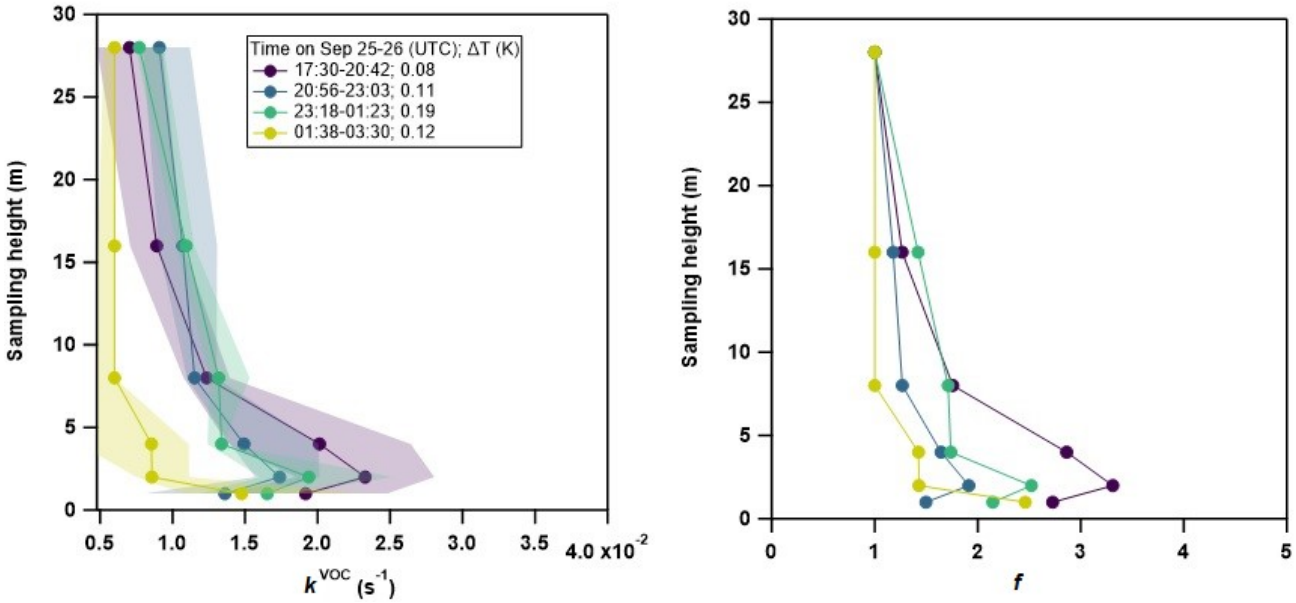

Figure S4: Median vertical profiles of VOC-induced NO_3 reactivity (k^{VOC}). The different time bins are coloured according to the legend that also includes the mean temperature inversions ($\Delta T = T_{27\ m} - T_{0.4\ m}$). Left panels: Height-resolved median profiles. The shaded areas indicate the 25th and 75th percentiles. Right panels: Fractional changes in NO_3 reactivity relative to 28 m (f, Eq. 1 in the main text) for the corresponding night types.

S5 Losses of NO_3 through heterogeneous reactions

The nitrate radical (NO_3) can be lost on particles either directly (k_{direct}) or indirectly ($k_{indirect}$) via the deposition of its equilibrium partner N_2O_5.[7] The overall pseudo first-order loss rate (k_{het}) of NO_3 on particles is:

$$k_{het} = k_{direct} + k_{indirect} = \frac{\gamma_{NO_3}\bar{c}_{NO_3}\,ASA}{4} + \frac{\gamma_{N_2O_5}\bar{c}_{N_2O_5}\,ASA}{4} K_{eq}[NO_2] \quad \text{(S6)}$$

with the heterogeneous uptake coefficients $\gamma_{N_2O_5}$ and γ_{NO_3} as well as the mean molecular velocities $\bar{c}_{N_2O_5}$ and $\bar{c}_{NO_3}$ of N_2O_5 and NO_3, respectively.[8] In order to assess the impact of these reactions, we used the aerosol number density and size-distribution measured next to the container area at a sampling height of 2 m to derive the aerosol surface area (ASA).[9] The term $K_{eq}[NO_2]$ was calculated from measured NO_2 mixing ratios and the equilibrium constant at the appropriate temperature.[10] We deployed a value of 0.03 for $\gamma_{N_2O_5}$ as reported for SOA in several studies.[11, 12] To assess an upper limit for the impact of k_{het} on the NO_3 radical budget, we chose a high value of 0.2 for γ_{NO_3} as reported for SOA originating from the nighttime oxidation of limonene.[13] The resulting values of k_{het} are depicted in Fig. S5. Despite the implementation of such a high value for γ_{NO_3}, k_{het} remains mostly below 0.003 s^{-1} and its campaign-median value is only 9.8×10^{-4} s^{-1}. This is negligible compared to a typical value of k^{VOC} = 0.04 s^{-1} during the day or during a coupled night (Fig. 5a).

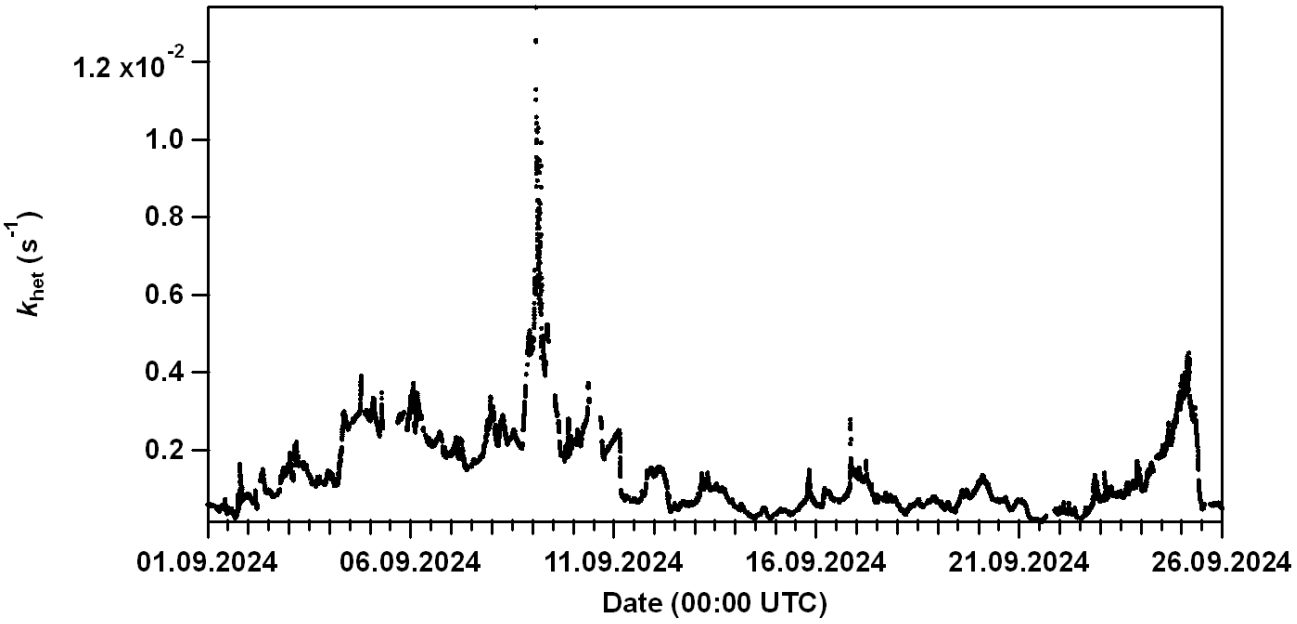

Figure S5: Overall pseudo first-order loss rate for NO_3 on particles (k_{het}) during the BAIRN-VIP as calculated with Eq. S6.

References

1. S. T. Andersen, C. Nelson, L. Wüst, P. Dewald, G. N. T. E. Türk, J. Schuladen, H. Fischer, M. Ehn, I. Ylivinkka, L. R. Ahonen, R. Rynek, H. Borsdorf, T. Mayer, J. Lelieveld and J. N. Crowley, Contribution of chemical reactions and deposition losses to the lifetimes and vertical gradients of O_3, PAN and PAA in a boreal forest, *submitted*, 2025.

2. O. Peltola, K. Lapo and C. K. Thomas, A Physics-Based Universal Indicator for Vertical Decoupling and Mixing Across Canopies Architectures and Dynamic Stabilities, *Geophys. Res. Lett.*, 2021, **48**, e2020GL091615.

3. O. Peltola, T. Aslan, M. Aurela, A. Lohila, I. Mammarella, D. Papale, C. K. Thomas, T. Vesala and T. Laurila, Towards an enhanced metric for detecting vertical flow decoupling in eddy covariance flux observations, *Agr. Forest Meteorol.*, 2025, **362**, 110326.

4. R. Stull, *Practical Meteorology: An Algebra-based Survey of Atmospheric Science*, University of British Columbia, Vancouver, 2017.

5. A. J. Dyer, A review of flux-profile relationships, *Bound.-Layer Meteorol.*, 1974, **7**, 363-372.

6. J. C. Kaimal and J. J. Finnigan, Oxford University Press, Oxford, 1994, DOI: 10.1093/oso/9780195062397.001.0001.

7. S. S. Brown and J. Stutz, Nighttime radical observations and chemistry, *Chem. Soc. Rev.*, 2012, **41**, 6405–6447.

8. J. M. Liebmann, J. B. A. Muller, D. Kubistin, A. Claude, R. Holla, C. Plaß-Dülmer, J. Lelieveld and J. N. Crowley, Direct measurements of NO_3-reactivity in and above the boundary layer of a mountain-top site: Identification of reactive trace gases and comparison with OH-reactivity, *Atmos. Chem. Phys.*, 2018, **18**, 12045-12059.

9. P. Aalto, K. Hämeri, E. Becker, R. Weber, J. Salm, J. M. Mäkelä, C. Hoell, C. D. O'dowd, H. Karlsson, H.-C. Hansson, M. Väkevä, I. K. Koponen, G. Buzorius and M. Kulmala, Physical characterization of aerosol particles during nucleation events, *Tellus B: Chemical and Physical Meteorology*, 2001, DOI: 10.3402/tellusb.v53i4.17127.

10. IUPAC: Task Group on Atmospheric Chemical Kinetic Data Evaluation, edited by: Ammann, M., Cox, R.A., Crowley, J.N., Herrmann, H., Jenkin, M.E., McNeill, V.F., Mellouki, A., Rossi, M. J., Troe, J. and Wallington, T. J., https://iupac.aeris-data.fr/en/home-english/, accessed 8 October 2025.

11. T. H. Bertram and J. A. Thornton, Toward a general parameterization of N_2O_5 reactivity on aqueous particles: the competing effects of particle liquid water, nitrate and chloride, *Atmos. Chem. Phys.*, 2009, **9**, 8351-8363.

12. G. J. Phillips, J. Thieser, M. J. Tang, N. Sobanski, G. Schuster, J. Fachinger, F. Drewnick, S. Borrmann, H. Bingemer, J. Lelieveld and J. N. Crowley, Estimating N_2O_5 uptake coefficients using ambient measurements of NO_3, N_2O_5, $ClNO_2$ and particle-phase nitrate, *Atmos. Chem. Phys.*, 2016, **16**, 13231-13249.

13. J. L. Fry, A. Kiendler-Scharr, A. W. Rollins, T. Brauers, S. S. Brown, H. P. Dorn, W. P. Dube, H. Fuchs, A. Mensah, F. Rohrer, R. Tillmann, A. Wahner, P. J. Wooldridge and R. C. Cohen, SOA from limonene: role of NO_3 in its generation and degradation, *Atmos. Chem. Phys.*, 2011, **11**, 3879-3894.